

Velocity-stress finite-difference modeling of poroelastic wave propagation

Shahin Moradi and Don C. Lawton

ABSTRACT

A velocity-stress staggered-grid 2D finite difference algorithm was developed in Matlab to model the wave propagation in poroelastic media. The Biot's equations of motion were formulated using a finite difference algorithm with fourth order accuracy in space and second order accuracy in time. We examined two examples, where the first was a single layer sandstone saturated with brine and CO_2 and second, a two-layered sandstone model with same matrix properties in both layers, but with different fluid content. As predicted by Biot's theory a slow compressional wave was observed in the particle velocity snapshots. In the layered model, at the boundary, the slow P-wave converts to a P-wave that travels faster than the slow P-wave. The results showed that our algorithm handles the layered model perfectly and should be examined for more complicated models. In the future, this finite difference algorithm could be used for inversion to obtain the properties of the porous media, such as saturation.

INTRODUCTION

Seismic modeling is an important part of the seismic inversion algorithm. In elastic seismic modeling the pore fluid properties such as density, velocity, viscosity and saturation are neglected in spite of the reservoir rocks being porous media saturated with fluids. Wave propagation in porous media has attracted attention in the last fifty years since Maurice Biot established his theory on poroelasticity (Biot, 1962). Biot's theory could be used in the oil and gas industry for exploration and monitoring purposes. It could also be used for detection of CO_2 at Carbon Capture and Storage projects where CO_2 is injected into deep geological formations for permanent storage. Wave propagation in a poroelastic media is more complicated than the elastic media due to the existence of pore fluid. The relative movement of the fluid with respect to the solid generates a second P-wave called "slow P-wave" which is strongly dissipative and has a velocity close to the velocity of the fluid. Numerical examination of the Biot's theory has been done in several ways (Carcione et al., 2010). Finite difference method is one of the most commonly used methods for numerical modeling. The Biot's equations have been formulated using various finite difference schemes. Zhu and McMechan (1991) used central-difference approximation to formulate the particle displacements. Others employed velocity-stress staggered-grid finite difference formulation (Dai et al., 1995; Sheen et al., 2006; Zeng and Liu, 2001).

In this study, we developed a velocity-stress finite difference algorithm in Matlab to model the wave propagation in the porous media. This algorithm can be used for inversion in the future to calculate the properties of the porous rock which are neglected in elastic modeling. In the next pages, the Biot's theory of poroelasticity will be briefly reviewed and the finite-difference formulation of the corresponding equations will be presented. At the end, the program is examined with numerical examples.

Biot's theory of poroelasticity

Maurice Biot was the first who established the theory of poroelasticity. He made the following assumptions to derive the equations of motion in the porous media: (1) the rock frame is assumed to be elastic; (2) the pores are connected so that the fluid could travel through the pore space; (3) the seismic wavelength is much larger than the average pore size; (4) the deformations are so small that the mechanical processes become linear; (5) the medium is statistically isotropic (Zhu and McMechan, 1991). Although Biot extended his theory to more general cases such as anisotropic porous media, in this work we concentrate on the isotropic case. The partial differential equations for the wave propagation in poroelastic media was also derived by Pride et al. (1992) using direct volume averaging.

From the stress-strain relation for a porous medium (Biot, 1962), the solid stress τ and the pore fluid pressure P are given by

$$\tau_{ij} = 2\mu e_{ij} + (\lambda_c e_{kk} + \alpha M \varepsilon_{kk})_{ij} \quad (1)$$

$$P = -\alpha M e_{kk} - M \varepsilon_{kk} \quad (2)$$

where $e_{ij} = \nabla \cdot u = \frac{1}{2}(\frac{\partial u_i}{\partial x_j} + \frac{\partial u_j}{\partial x_i})$ is the solid strain, with u being the particle velocity of the solid, and $\varepsilon_{ij} = \nabla \cdot (u - U)$, where U is the particle displacement of the fluid. μ is the shear modulus and λ_c is the Lamé parameter of the saturated rock. α is defined by $1 - \frac{K_{Dry}}{K_{Solid}}$ where K_{Solid} and K_{Dry} are the bulk moduli of the solid and the dry rock frame, respectively. M is coupling modulus defined by $[\frac{\phi}{K_{Fluid}} + \frac{(\alpha - \phi)}{K_{Solid}}]$, with K_{Fluid} being the bulk modulus of the fluid.

In addition, based on Biot's theory, equations of motion for a statistically isotropic porous media saturated with viscous fluid are:

$$(m\rho - \rho_f^2) \frac{\partial^2 u_i}{\partial t^2} = m \frac{\partial \tau_{ij}}{\partial x_j} + \rho_f b \frac{\partial w_i}{\partial t} + \rho_f \frac{\partial P}{\partial x_i} \quad (3)$$

$$(m\rho - \rho_f^2) \frac{\partial^2 w_i}{\partial t^2} = -\rho_f \frac{\partial \tau_{ij}}{\partial x_j} - \rho b \frac{\partial w_i}{\partial t} - \rho \frac{\partial P}{\partial x_i} \quad (4)$$

where $w = u - U$ is the particle displacement vector of the fluid relative to the solid. ρ_f and ρ are the fluid and saturated rock densities and b is the fluid mobility defined by η/κ , with η being the viscosity of the fluid and κ being the permeability of the porous rock. $m = T \frac{\rho_f}{\phi}$ is the effective density of the fluid, with T being the tortuosity. Equations (3) and (4) are second order differential equations in time. By defining the solid and relative particle velocities $V = \frac{\partial u}{\partial t}$ and $W = \frac{\partial w}{\partial t}$ these equations could be written as first order equations in time:

$$(m\rho - \rho_f^2) \frac{\partial V_i}{\partial t} = m \frac{\partial \tau_{ij}}{\partial x_j} + \rho_f b W + \rho_f \frac{\partial P}{\partial x_i} \quad (5)$$

$$(m\rho - \rho_f^2) \frac{\partial W_i}{\partial t} = -\rho_f \frac{\partial \tau_{ij}}{\partial x_j} - \rho b W - \rho \frac{\partial P}{\partial x_i} \quad (6)$$

Furthermore, by taking derivatives with respect to time from both sides of equations (1) and (2) we will have:

$$\frac{\partial \tau_{ij}}{\partial t} = 2\mu \frac{\partial e_{ij}}{\partial t} + (\lambda_c \frac{\partial e_{kk}}{\partial t} + \alpha M \frac{\partial \varepsilon_{kk}}{\partial t}) \delta_{ij} \quad (7)$$

$$\frac{\partial P}{\partial t} = -\alpha M \frac{\partial e_{kk}}{\partial t} - M \frac{\partial \varepsilon_{kk}}{\partial t} \quad (8)$$

In the 2D case, equations (5), (6), (7) and (8) make a set of 8 coupled equations which can be used for finite difference modeling. These equations are:

$$\frac{\partial \tau_{xx}}{\partial t} = (\lambda_c + 2\mu) \frac{\partial V_x}{\partial x} + \lambda_c \left(\frac{\partial V_z}{\partial z} \right) + \alpha M \left(\frac{\partial W_x}{\partial x} + \frac{\partial W_z}{\partial z} \right) \quad (9)$$

$$\frac{\partial \tau_{zz}}{\partial t} = (\lambda_c + 2\mu) \frac{\partial V_z}{\partial z} + \lambda_c \left(\frac{\partial V_x}{\partial x} \right) + \alpha M \left(\frac{\partial W_x}{\partial x} + \frac{\partial W_z}{\partial z} \right) \quad (10)$$

$$\frac{\partial \tau_{xz}}{\partial t} = \mu \left(\frac{\partial V_z}{\partial x} + \frac{\partial V_x}{\partial z} \right) \quad (11)$$

$$\frac{\partial P}{\partial t} = -\alpha M \left(\frac{\partial V_x}{\partial x} + \frac{\partial V_z}{\partial z} \right) - M \left(\frac{\partial W_x}{\partial x} + \frac{\partial W_z}{\partial z} \right) \quad (12)$$

$$\frac{\partial V_x}{\partial t} = A \left(\frac{\partial \tau_{xx}}{\partial x} + \frac{\partial \tau_{xz}}{\partial z} \right) + B W_x + C \frac{\partial P}{\partial x} \quad (13)$$

$$\frac{\partial V_z}{\partial t} = A \left(\frac{\partial \tau_{zx}}{\partial x} + \frac{\partial \tau_{zz}}{\partial z} \right) + B W_z + C \frac{\partial P}{\partial z} \quad (14)$$

$$\frac{\partial W_x}{\partial t} = D \left(\frac{\partial \tau_{xx}}{\partial x} + \frac{\partial \tau_{xz}}{\partial z} \right) + E W_x + F \frac{\partial P}{\partial x} \quad (15)$$

$$\frac{\partial W_z}{\partial t} = D \left(\frac{\partial \tau_{zx}}{\partial x} + \frac{\partial \tau_{zz}}{\partial z} \right) + E W_z + F \frac{\partial P}{\partial z} \quad (16)$$

where $A = \frac{m}{(m\rho - \rho_f^2)}$, $B = \frac{\rho_f b}{(\rho - \rho_f^2)}$, $C = \frac{\rho_f}{(m\rho - \rho_f^2)}$, $D = \frac{-\rho_f}{(m\rho - \rho_f^2)}$, $E = \frac{-\rho b}{(m\rho - \rho_f^2)}$ and $F = \frac{-\rho}{(m\rho - \rho_f^2)}$. These stress-particle velocity equations can be used for finite difference modeling using staggered-grid scheme.

Staggered-grid finite difference algorithm

To model the wave propagation in poroelastic media, equations (9) to (16) need to be discretized using the finite difference algorithm. The unknowns are the solid stresses τ_{xx}, τ_{zz} and τ_{xz} , the fluid pressure P , the solid particle velocities V_x and V_z , and the fluid particle velocities W_x and W_z . For more accuracy a velocity-stress staggered-grid finite difference scheme was used for numerical modeling. In this scheme the solid stresses τ_{xx}, τ_{zz} and the fluid pressure P , are calculated on the regular grid whereas other unknowns are calculated on the staggered grid where the grid points are shifted by half a grid size (Figure 1).

By discretizing the differential equations (9) to (16) using the staggered-grid scheme we have:

$$V_{x^{i+1/2},j}^{n+1/2} = V_{x^{i+1/2},j}^{n-1/2} + \Delta t [A(\Delta_x \tau_{xx} + \Delta_z \tau_{xz}) + C \frac{\partial P}{\partial x}]_{i+1/2,j}^n + B \Delta t W_{x^{i+1/2},j}^{n-1/2} \quad (17)$$

$$V_{z^{i,j+1/2}}^{n+1/2} = V_{z^{i,j+1/2}}^{n-1/2} + \Delta t [A(\Delta_x \tau_{xz} + \Delta_z \tau_{zz}) + C \frac{\partial P}{\partial z}]_{i,j+1/2}^n + B \Delta t W_{z^{i,j+1/2}}^{n-1/2} \quad (18)$$

$$W_{x^{i+1/2,j}}^{n+1/2} = W_{x^{i+1/2,j}}^{n-1/2} + \Delta t [D(\Delta_x \tau_{xx} + \Delta_z \tau_{xz}) + F \frac{\partial P}{\partial x}]_{i+1/2,j}^n + E \Delta t W_{x^{i+1/2,j}}^{n-1/2} \quad (19)$$

$$W_{z^{i,j+1/2}}^{n+1/2} = W_{z^{i,j+1/2}}^{n-1/2} + \Delta t [D(\Delta_x \tau_{xz} + \Delta_z \tau_{zz}) + F \frac{\partial P}{\partial z}]_{i,j+1/2}^n + E \Delta t W_{z^{i,j+1/2}}^{n-1/2} \quad (20)$$

$$\tau_{xx^{i,j}}^{n+1} = \tau_{xx^{i,j}}^n + \Delta t [(\lambda_c + 2\mu) \Delta_x V_x + \lambda_c \Delta_z V_z + \alpha M(\Delta_x W_x + \Delta_z W_z)]_{i,j}^{n+1/2} \quad (21)$$

$$\tau_{zz^{i,j}}^{n+1} = \tau_{zz^{i,j}}^n + \Delta t [(\lambda_c + 2\mu) \Delta_z V_z + \lambda_c \Delta_x V_x + \alpha M(\Delta_x W_x + \Delta_z W_z)]_{i,j}^{n+1/2} \quad (22)$$

$$\tau_{xz^{i+1/2,j+1/2}}^{n+1} = \tau_{xz^{i+1/2,j+1/2}}^n + \Delta t [\mu(\Delta_x V_z + \Delta_z V_x)]_{i+1/2,j+1/2}^{n+1/2} \quad (23)$$

$$P_{i,j}^{n+1} = P_{i,j}^n - \Delta t [\alpha M(\Delta_x V_x + \Delta_z V_z) + M(\Delta_x W_x + \Delta_z W_z)]_{i,j}^{n+1/2} \quad (24)$$

where superscripts and subscripts denote temporal and spatial indices, respectively. At any time t , $t = t_0 + n\Delta t$, where t_0 is the initial time and Δt is the temporal sampling. At location (x, z) , $x = x_0 + ih$ and $z = z_0 + jh$, where (x_0, z_0) is the initial location, and h is the spatial sampling. Δ_x and Δ_z are fourth-order $O(h^4)$ partial differential operators with respect to x and z , that are centred about the quantity being calculated (Levander, 1988). For example :

$$\Delta_x V_x|_{i,j}^{n+1/2} = [-c_2(V_{x^{i+1/2}}^{n+1/2} - V_{x^{i-1/2}}^{n+1/2}) - c_1(V_{x^{i+3/2}}^{n+1/2} - V_{x^{i-3/2}}^{n+1/2})]/h \quad (25)$$

where $c_2 = 9/8$ and $c_1 = 1/24$, are the inner and outer difference coefficients defined by Levander (1988).

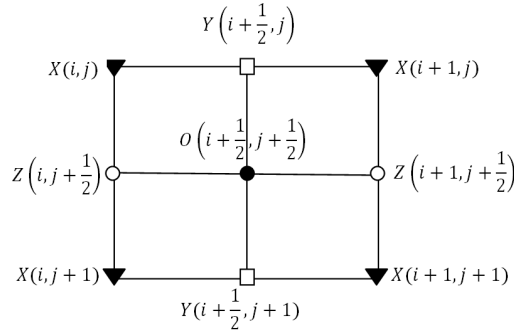


FIG. 1. The staggered-grid layout and the locations of stress, velocity and pressure components. In this diagram τ_{xx}, τ_{zz} and P are marked by X, V_x and W_x by Y, V_z and W_z by Z, and τ_{xz} by O.

Numerical examples and analysis

Equations (17) to (24) were programmed in Matlab to simulate the wave propagation in a homogenous, isotropic, poroelastic media. To examine this program, two models were defined based on the Quest Carbon Capture and Storage project in Alberta. The purpose of the Quest project is to reduce the CO_2 emission from Scotford Upgrader by storing CO_2 in a deep geological formation (Shell, 2010). The location of the Scotford

Upgrader is about 5 km northeast of Fort Saskatchewan, Alberta, within an industrial zone. The selected geological formation for the CO_2 storage is Basal Cambrian Sands or BCS, which is a saline aquifer within the Western Canadian Sedimentary Basin (WCSB) with an approximate depth of 2000 m from the surface. The first numerical example used in this study was a single layer model generated using the properties of the storage formation, BCS. The rock properties of the BCS were obtained from the log data available at the area of study (Moradi and Lawton, 2012). The purpose was to have a model of BCS after injecting the CO_2 . Change of the pore fluid leads to the change in the physical properties of the rock including the P-wave velocity and the density (Gassmann, 1951; Smith et al., 2003). In order to calculate these changes, Gassmann fluid substitution modeling was undertaken for BCS using the Gassmann method (Moradi and Lawton, 2012). Figure 2 shows the changes of the P-wave velocity in BCS versus the CO_2 saturation. Note that the velocity changes rapidly for the saturation values below 20% and gradually for values above 20%. The maximum change occurs between values of 40% to 45% CO_2 saturation. Therefore our single layer model was a porous sandstone saturated with a mixture of brine and CO_2 where CO_2 saturation was chosen to be 40%. The properties of this model are listed in Table 1.

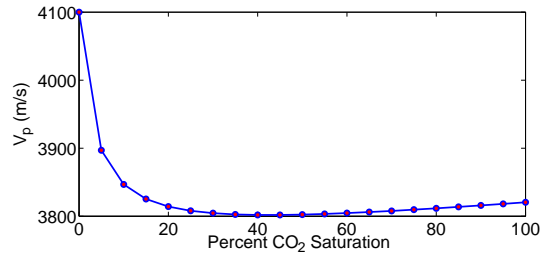


FIG. 2. The Change in P-wave velocity in the BCS after injecting CO_2 . The maximum change occurs at 40% saturation.

Table 1. Physical properties of the example models

	Single layer model	Two layer model	
		Layer one	Layer two
ρ_f	937 (kg/m^3)	1070 (kg/m^3)	937 (kg/m^3)
ρ	2370 (kg/m^3)	2400 (kg/m^3)	2370 (kg/m^3)
V_p	3800 (m/s)	4100 (m/s)	3800 (m/s)
V_s	2400 (m/s)	2390 (m/s)	2400 (m/s)
ϕ	16%	16%	16%
κ	1(mD)	1(mD)	1(mD)
η	0.001($Poise$)	0.003($Poise$)	0.001($Poise$)

The stability condition is the same as the one in the elastic case (Zhu and McMechan, 1991):

$$\Delta t \leq \frac{h}{(V_p^2 - V_s^2)^{1/2}} \quad (26)$$

where V_p and V_s are the compressional and shear wave velocities of the saturated rock. However this condition can be used only for the internal grid, and for the boundary condition a different condition must be used (Kamel, 1989).

Snapshots of the particle velocities were then calculated for this single layer model. A ricker wavelet with the dominant frequency of 50 Hz was used as the source. To inject the explosive source into the medium, the wavelet was added to the normal solid stresses and fluid pressure. For this purpose, the source was weighted by a factor of ϕ for the fluid pressure and by a factor of $(1 - \phi)$ for the solid normal stresses, with ϕ being the porosity of the rock. The size of the model was $1500m$ by $1500m$ and the source was located at the centre of the model, $(x, z) = (750, 750)m$. The grid spacings chosen for this example were $dx = dz = 3m$, and the time step was $dt = 0.2 ms$.

The calculated snapshots for the vertical particle velocities of the fluid and solid are shown in Figure 3. As predicted by Biot's theory, there are two P-waves traveling in the medium where the Slow P-wave travels with a speed close to the wave speed in the fluid. The particle velocity of the slow P-wave in the solid is out of phase with the one in the fluid. In contrast, for the fast P-wave the particle velocities are in phase in the solid and fluid.

Figure 4 shows the fluid pressure snapshots for this model. The slow P-wave has a larger relative amplitude than the fast P-wave which is because the slow P-wave is originated from the fluid movement.

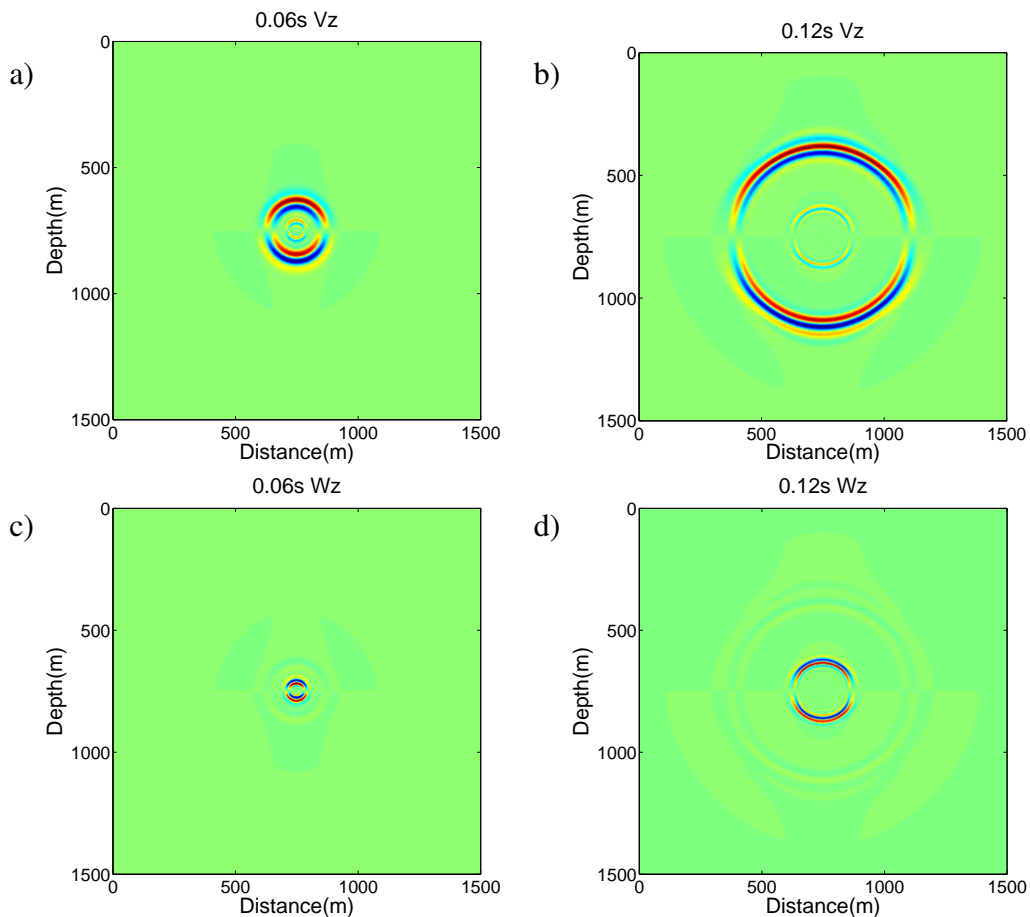


FIG. 3. The snapshots for the vertical particle velocities of the solid (a and b), and the fluid with respect to the solid (c and d) at times 0.06 s and 0.12 s.

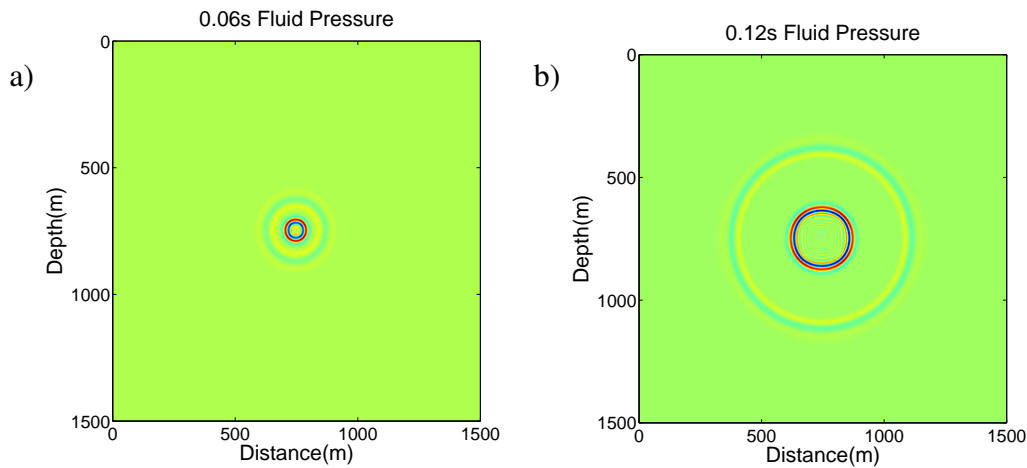


FIG. 4. The snapshots of the fluid pressure at times 0.06 s and 0.12 s.

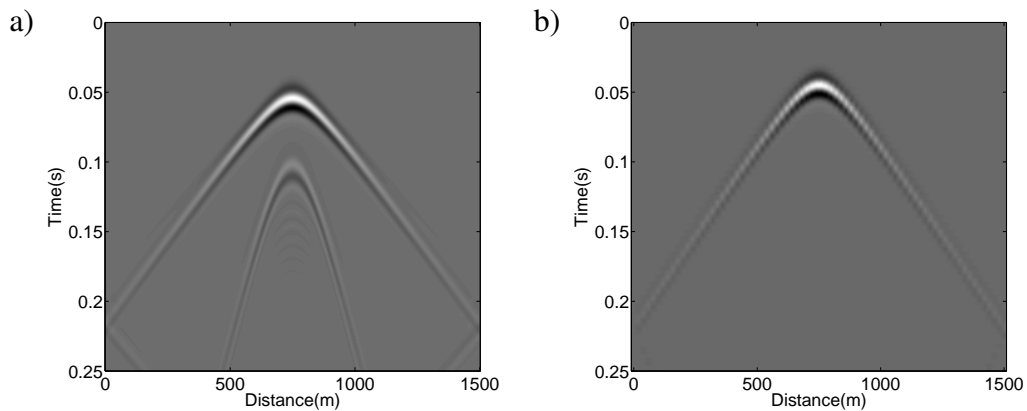


FIG. 5. Comparison between Poroelastic FD algorithm(a) and the elastic FD algorithm(b)

The poroelastic algorithm was then compared with the elastic one by generating shot gathers from both algorithms. The elastic shot gathers were generated by mFD2D program from the CREWES Matlab toolbox. The parameters and the grid size were the same as before and the receiver line was at the depth of $z = 600 \text{ m}$. The generated shot gathers for both algorithms are shown in Figure 5. As observed from the snapshots, the slow P-wave is apparent in the poroelastic shot gather. The comparison between these two shot gathers shows that our algorithm is consistent with the elastic one, except in the poroelastic algorithm there is a slow P-wave that elastic algorithm does not generate.

Another example used in this study was a 2-layer model which was also based on the Quest project. In this 2-layer model, the top layer was, a sandstone with the properties of BCS before injecting CO_2 with the pore fluid being brine, and the lower layer was the same layer used in the previous example as a single layer. This model represents a sandstone with different pore fluid at the top and the bottom of the rock. The properties of this model are listed in Table 1. The size of the model, the grid spacing and the time step were the same as those in the previous example. In this example the source was located at $(x, z) = (750, 650) \text{ m}$, and the receiver line was at the depth of 600 m . Figure 6a shows

this model with a boundary at the depth of 750 m. The vertical particle velocity snapshot calculated for this model is shown in Figure 6b.

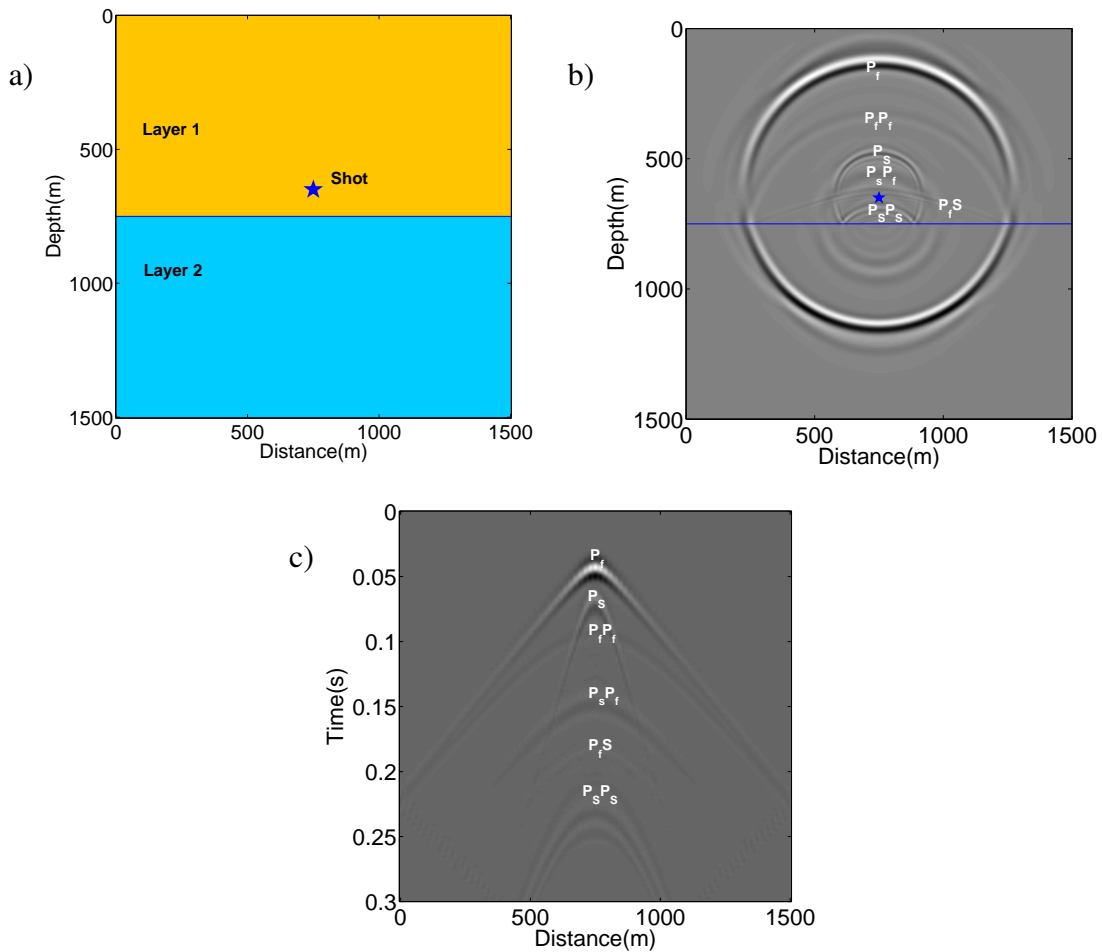


FIG. 6. The 2-layer model used as a numerical example(a), The solid vertical particle velocity snapshot calculated for this model at the time 0.16 s (b), and the corresponding shot gather.

This figure shows several wave modes including the converted waves. P_f and P_s denote the fast and the slow P-waves, respectively. $P_f P_f$ is the reflected fast P-wave, $P_s P_s$ is the reflected slow P-wave, and $P_f S$ is the reflected S-wave that is converted from a fast P-wave. A reflected fast P-wave which is converted from the slow P-wave is also evident in this figure. This wave which is marked as $P_s P_f$, travels faster than the slow P-wave. The arrivals are shown in the corresponding shot gather, in Figure 6c. As discussed earlier, an elastic algorithm does not generate the slow P-wave or any converted waves from this wave mode, for instance $P_s P_f$ and $P_s P_s$. However, poroelastic modeling could give us information about the fluid content of the rock which is of interest in CO_2 injection, and oil and gas exploration.

CONCLUSION

Biot's equations of motion were programmed in Matlab using a velocity-stress staggered grid finite-difference algorithm to simulate wave propagation in poroelastic media. As a numerical example we used a single layer model of a sandstone saturated with a mixture of brine and CO_2 to generate the snapshots of the particle velocities and the fluid pressure. As predicted by Biot's theory, two compressional waves appeared in the snapshots of the particle velocities. A 2-layered model was also examined to see the wave behaviour at a boundary. This model had two layers with the same matrix properties but with different pore fluids. The calculated vertical particle velocity showed different wave modes generated at the boundary including a fast P-wave which is converted from the slow P-wave. This poroelastic FD algorithm could be used in the future for inversion to obtain porous media properties that are ignored in elastic algorithms.

ACKNOWLEDGMENTS

We thank Carbon Management Canada (CMC) for financial support of this research and the CREWES project for extensive technical support. Hassan Khaniani, Peter Manning and Joe Wong, from CREWES, and also David Aldridge from Sandia National Laboratories are thanked for their helpful comments and discussions.

REFERENCES

- Biot, M. A., 1962, Mechanics of deformation and acoustic propagation in porous media: *Journal of Applied Physics*, **33**, 1482–1498.
- Carcione, J. M., Morency, C., and Santos, J. E., 2010, Computational poroelasticity-a review: *Geophysics*, **75**, No. 5, 75A229–75A243.
- Dai, N., Vafidis, A., and Kanasevich, E., 1995, Wave propagation in heterogeneous, porous media: a velocity-stress, finite-difference method: *Geophysics*, **60**, 327–340.
- Gassmann, F., 1951, Über die elastizität poroser medien: *Vierteljahresschrift der Naturforschenden Gesellschaft in Zurich*, **96**, 1–23.
- Kamel, A. H., 1989, A stability checking procedure for finite-difference schemes with boundary conditions in acoustic media: *Bull. Seis. Soc. Am.*, **79**, 1601–1606.
- Levander, A. R., 1988, Fourth-order finite-difference p-sv seismograms: *Geophysics*, **53**, No. 11, 1425–1436.
- Moradi, S., and Lawton, D. C., 2012, Time lapse seismic monitoring of CO_2 sequestration at quest ccs project: CREWES Research Report, **24**.
- Pride, S. R., Gangi, A., and Morgan, F., 1992, Deriving the equations of motion for porous isotropic media: *The Journal of Acoustical Society of America*, **92**, 3278–3290.
- Sheen, D. H., Tuncay, K., Baag, C., and Ortoleva, P., 2006, Parallel implementation of a velocity-stress staggered-grid finite-difference method for 2-d poroelastic wave propagation: *Computers and Geosciences*, **32**, 1182–1191.
- Shell, 2010, Quest carbon capture and storage project: Project description, **1**.
- Smith, T., Sondergeld, C., and Rai, C. S., 2003, Gassmann fluid substitutions: A tutorial: *Geophysics*, **68**, No. 2, 430–440.

- Zeng, Y., and Liu, Q., 2001, The application of the perfectly matched layer in numerical modeling of wave propagation in poroelastic media: *Geophysics*, **66**, No. 4, 1258–1266.
- Zhu, X., and McMechan, A., 1991, Numerical simulation of seismic responses of poroelastic reservoirs using biot's theory: *Geophysics*, **56**, No. 3, 328–339.